

Multiwalled carbon nanotubes grown in hydrogen atmosphere: An x-ray diffraction study

Yutaka Maniwa,¹ Ryuji Fujiwara,¹ Hiroshi Kira,¹ Hideki Tou,¹ Eiji Nishibori,² Masaki Takata,² Makoto Sakata,² Akihiko Fujiwara,³ Xinluo Zhao,⁴ Sumio Iijima,^{4,5} and Yoshinori Ando⁵

¹Department of Physics, Tokyo Metropolitan University, Minami-osawa, Hachi-oji, Tokyo 192-0397, Japan

²Department of Applied Physics, Nagoya University, Nagaya 464-8603, Japan

³Department of Physics, School of Science, University of Tokyo, 7-3-1 Hongo, Bunkyo-ku, Tokyo 113, Japan

⁴JST-ICORP Nanotubulite Project, Japan

⁵Department of Materials Science and Engineering, Meijyo University, Tempaku-ku, Nagoya 468-8502, Japan

(Received 11 April 2001; published 25 July 2001)

X-ray diffraction study of multiwalled carbon nanotube (MWNT) grown by arc discharge in hydrogen atmosphere is presented. It is found that the thermal-expansion coefficient along the radial direction of MWNT is widely distributed in a range from $1.6 \times 10^{-5} \text{ K}^{-1}$ to $2.6 \times 10^{-5} \text{ K}^{-1}$, indicating the existence of both of Russian doll MWNT and highly defective MWNT. Russian doll MWNT is suggested to have the outer diameter less than $\sim 100 \text{ \AA}$. Thicker MWNT's are typically highly defective, and may have the jelly roll (scroll) or defective polygonal structure consisting of flat graphite domains.

DOI: 10.1103/PhysRevB.64.073105

PACS number(s): 61.10.Dp, 61.43.-j, 68.37.Lp

Since Iijima¹ found carbon nanotubes in deposits after arc discharge of carbon rod, extensive studies on its structure have been reported.² In single-walled carbon nanotube (SWNT) with a typical diameter of 14 \AA ,^{3,4} the Raman spectra exhibited radial breathing mode (RBM) whose frequency sensitively depends on the tube diameter.^{5,6} The scanning tunneling spectroscopy (STS) for the individual SWNT confirmed the predicted one-dimensional electronic structure.^{7,8} Such observations are consistent with a closed seamless tubular structure made of graphene sheet. On the other hand, the structure of multiwalled carbon nanotube (MWNT) (Refs. 1 and 2) with many separated "concentric" tubules is rather uncertain. This is a serious problem because the topology of the carbon network governs the electronic structure. In this paper, we present an evidence for the existence of MWNT consisting of seamless tubules in materials grown in a hydrogen atmosphere.

The transmission electron microscopy (TEM) images of MWNT usually indicate closed concentric (or the so-called "Russian doll") tubular structure as shown in Fig. 1(a). However, it was claimed that the Russian doll structure is sometimes difficult to distinguish from the scroll-type (so-called "jelly roll") structures in Fig. 1(b).⁹ The scroll-type tubules have also been reported to really exist in MWNT materials grown by arc discharge.¹⁰ The interlayer compressibility⁹ and thermal-expansion coefficient¹¹ studied by an x-ray diffraction (XRD) were comparable to those of the graphite interlayer spacing, against an expectation that an ideal Russian doll MWNT should have very small thermal expansion and compressibility owing to the strong in-plane carbon-carbon bond. This observation strongly suggested that the bulk materials studied are essentially the scroll-type or highly defective MWNT's.

Very recently, Zhao and Ando¹² and Kataura *et al.*¹³ succeeded in the observation of RBM in MWNT. Although the typical inner diameter of the ordinal MWNT is usually too large to observe RBM, the sample grown by arc discharge in a hydrogen atmosphere (Ando's MWNT) was found to contain MWNT's with smaller inner diameter $< 10 \text{ \AA}$.^{12,14,15}

Therefore we expected that RBM's originating from the inner tubules should be observed in this sample. Although the RBM's corresponding to the innermost tubules were actually observed, those for the larger tubules (for example, the second layer tubules) were missing. Thus we investigated the materials by an XRD as a function of temperature in order to obtain further information on the structure.

XRD measurements were performed using synchrotron radiation source at SPring-8 beam-line BL02B2. The powder XRD patterns were collected using a powder x-ray diffractometer equipped with an imaging plate (IP) of $25 \times 40 \text{ cm}$ with a resolution of 100 \mu m . The x-ray wavelength was 0.9942 \AA . The samples were sealed in quartz capillary. A heat-gun-type temperature-control unit (Rigaku Ltd.) was used to control the sample temperature in a range from room temperature (RT) to 900 K . The detailed sample preparation and characterization by TEM and scanning electron microscopy (SEM) have been described in previous papers.¹²⁻¹⁵

Figure 2(a) shows the powder XRD profiles as a function of temperature. The result of the empty quartz capillary was also shown. Here, the wave vector transfer Q is defined by $(4\pi \sin \Theta)/\lambda$ where 2Θ is the scattering angle and λ is the wavelength. The peaks are indexed on the basis of the hexagonal graphite as indicated. The peak $(00l)$ and $(hk0)$ imply the interplane and in-plane reflections, respectively. In addition, comparing to the empty capillary, we found that the sample causes the large reflection below $Q=0.6 \text{ (\AA}^{-1}\text{)}$.

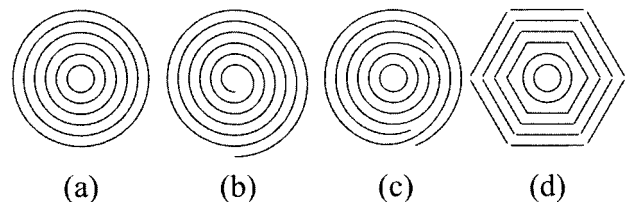


FIG. 1. Cross sections of (a) concentric (Russian doll) MWNT, (b) scroll (jellyroll) MWNT, (c) mixed MWNT of Russian doll and jellyroll structures proposed by Amelinckx *et al.*, and (d) polyhedral graphite tube with defects at the ridges.

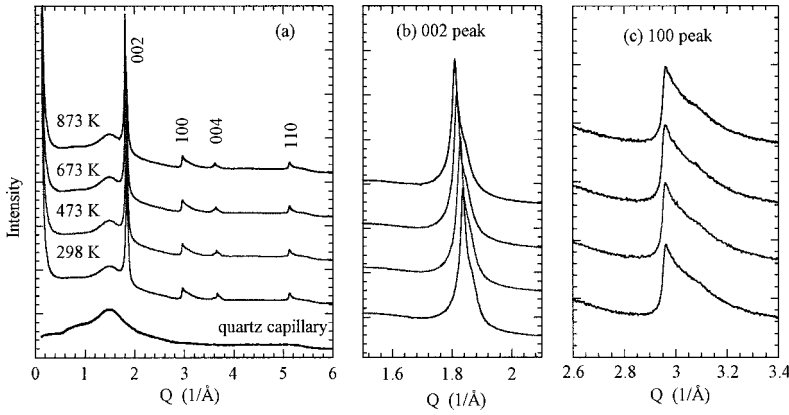


FIG. 2. (a) XRD patterns of Ando's MWNT at several temperatures, along with that of an empty quartz capillary. (b) and (c) are the expanded views of the (002) and (100) reflection peaks. The x-ray wavelength is 0.9942 Å.

This is due to a small angle scattering emanating from thin tubules and nanoparticles in the sample.

From the expanded view for the (002) reflection in Fig. 2(b), it is known that the peak position significantly shifts to the low- Q side on heating. On the other hand, the (100) peak does not change by elevating temperature (T) [Fig. 2(c)]. The difference in T dependence of the peak position between the (002) and (100) peaks implies that the in-plane thermal expansion is negligibly small compared to that for the interlayer spacing. We also noticed a strong asymmetry, “saw-tooth” shape, for the (100) peak. This is a characteristic of turbostratic graphite lacking interlayer stacking correlation.¹⁶ The same results were obtained by lowering T to RT. Therefore the sample was preserved by the present sample treatment.

For a quantitative discussion, we plotted the T dependence of the interlayer spacing estimated from the (100) and (00 l) peak positions, $d_{100}(T)$ and $d_{00l}(T)$ normalized at RT in Fig. 3. The thermal-expansion coefficient was obtained as $\alpha_{00l} = (2.6 \pm 0.2) \times 10^{-5} \text{ K}^{-1}$ for d_{00l} and $\alpha_{100} = (0 \pm 0.1) \times 10^{-5} \text{ K}^{-1}$ for d_{100} . The observed interlayer coefficient α_{00l} is comparable to $2.58 \times 10^{-5} \text{ K}^{-1}$ for HOPG (Ref. 17) and the previously reported value for MWNT.¹¹ In the case of Russian doll MWNT, the α_{00l} should be determined by the

strong in-plane carbon-carbon bonds, so that we expect $\alpha_{00l} \sim \alpha_{100}$. On the other hand, in the case of scroll type MWNT, α_{00l} and α_{100} are independent of each other, and we naturally expect $\alpha_{00l} \gg \alpha_{100}$ similar to the case of graphite. Therefore we may conclude from the above results that the majority of Ando's MWNT materials has highly defective or jellyroll-type structure, which supports the previous conclusions.^{9,11} However, the sample may be a mixture of these two types of MWNT. Hence we analyzed the (00 l) peak in more detail.

First, we discuss the source of (00 l) peak width, essentially in the same way as reported by Reznik *et al.*¹⁸ There are two possible sources for the peak broadening. One is due to the coherent length corresponding to the tube diameter; this is the so-called *domain size broadening*. For this case,¹⁸ the full width at half maximum (FWHM) is independent of the reflection index l as follows:

$$\Delta Q_{\text{size}} = 2(\pi \ln 2)^{1/2} \frac{1}{Nd},$$

where N is the number of layers (tubules) and d is the interlayer spacing. The other possible source is the distribution of d spacing (the so-called *strain broadening*). For this case, the FWHM is given by

$$\Delta Q_s = \frac{\pi l}{d^2} \Delta d,$$

where Δd is the FWHM of the distribution of interlayer spacing. Because both the sources differently depend on the index l , we can separate these two contributions by a comparison between the (002) and the (004) reflection. Experimentally, the (00 l) peak width was found to be nearly proportional to the index l . As shown in the inset of Fig. 4, the (004) peak is found to be well reproduced by the (002) peak, if the Q value for the (002) peak is multiplied by factor 2 and the intensity is normalized at the peak position. Therefore it is said that the broadening is dominated by the distribution of d spacing.

Now we can discuss the thermal expansion along the radial direction in details. Figure 4(a) shows the (002) reflection at RT (298 K) and 873 K. Here the Q value for the 873-K data was multiplied by $(1 + \alpha \Delta T)$ where $\Delta T = 575 \text{ K}$ is the temperature difference. For this scaling, the

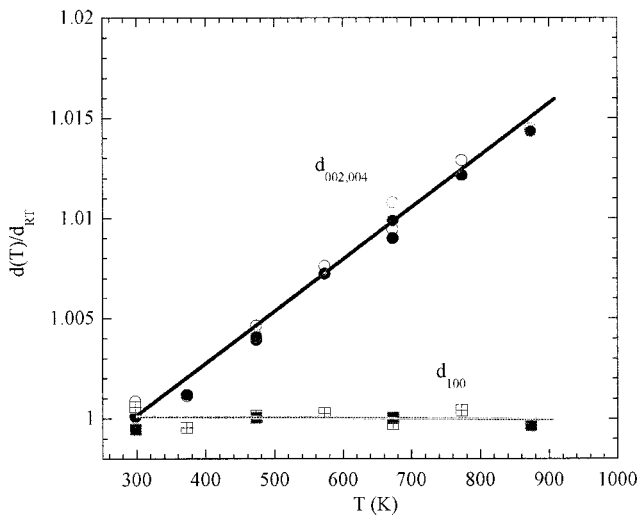


FIG. 3. Temperature dependence of interplane and in-plane d spacing normalized at 298 K in Ando's MWNT.

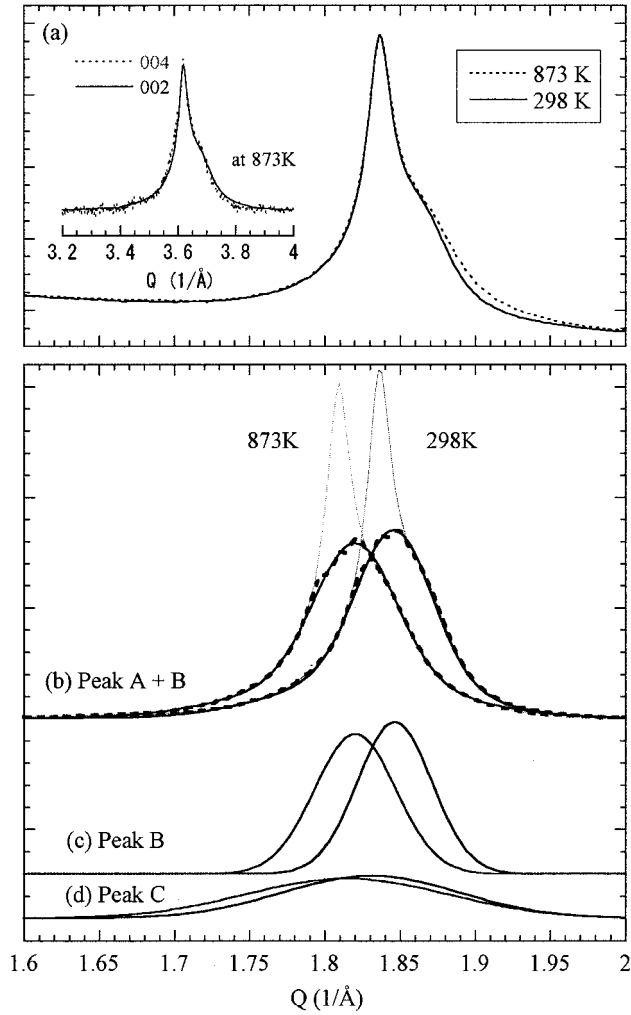


FIG. 4. (a): the (002) peaks at 298 K (solid line) and 873 K (dotted line). The Q value for the data taken at 878 K was multiplied by $(1 + \Delta\alpha T)$ where $\alpha = 2.6 \times 10^{-5}$ (1/K) and $\Delta T = 575$ K. The intensity is normalized at the peak. Inset to (a): a comparison between the (002) and (004) peaks of the 873-K data, where the Q for the (002) peak was multiplied by factor 2. The background reflection was subtracted and the peak intensity is normalized at the peak position. (b) The experimental data subtracted by the background reflection (thin solid line). The dotted line shows the data subtracted by peak A and the background reflection. The thick solid line is the sum of simulated peaks B and C. (c) and (d) Simulated components for peaks B and C, respectively.

peak position becomes T independent when all the materials have the same α , because the Bragg condition is given by $1 = 2d \sin \Theta / \lambda = (1 + \alpha \Delta T) d(RT) Q / 2\pi$, where $d(RT)$ is the interlayer spacing at 298 K. Actually, if we take $\alpha = 2.6 \times 10^{-5} \text{ K}^{-1}$, the peaks coincide well with each other as shown in Fig. 4(a), except for the high- Q tail. Because the peak profile directly reflects the d spacing through Bragg condition $d = 2\pi/Q$, the disagreement at high Q clearly indicates the existence of materials having α value which is smaller than $2.6 \times 10^{-5} \text{ K}^{-1}$.

For further discussion, we decomposed the observed (002) peak into several components with different α . It was found that at least three components (A, B, and C) are required to reproduce the observed (002) reflection, when symmetrical line shape is assumed for each component. In Table I, we have summarized the obtained fitting parameters using Gaussian line shape for each component, $\exp[-(Q - Q_i)^2 / \Delta Q_i^2]$ where Q_i is the Bragg position, ΔQ_i the linewidth, and $i = A, B,$ and C . One of them (peak A) reproduces a sharp structure peaked at the low Q side. The dotted line in Fig. 4(b) shows the data subtracted by the peak A from the raw data (thin line) after subtracting the background intensity. It is important to note that the intensity of the broadest peak C is T independent. Therefore the so-called thermal diffuse scattering (TDS), which usually appears as a broad peak around the Bragg peak and grows up with increasing T , is ruled out for the origin of peak C.

The averaged interlayer thermal-expansion coefficient α is obtained from the peak positions at RT and 873 K. For peaks A and B, α is $\sim 2.6 \times 10^{-5} \text{ K}^{-1}$ comparable to the graphite, while $1.6 \times 10^{-5} \text{ K}^{-1}$ for peak C. Therefore peaks A and B should be assigned to the highly defective MWNT, and peak C is most probably due to the Russian-doll-type structure. However, the observed α for peak C is substantially larger than the expected one for the ideal Russian doll MWNT, $\alpha = \alpha_{100} = (0 \pm 0.1) \times 10^{-5} \text{ K}^{-1}$. To explain the difference, we have two likely models based on a fact that the observed α is an averaged value over the sample material. One is that there are two types of MWNT contributing to the peak C, i.e., the Russian-doll-type MWNT with $\alpha \sim 0 \times 10^{-5} \text{ K}^{-1}$ and the highly defective MWNT with $\alpha \sim 2.6 \times 10^{-5} \text{ K}^{-1}$. Assuming that the observed α is weight-averaged corresponding to the content of both types of the MWNT's, the amount of the Russian doll MWNT is esti-

TABLE I. The (002) peaks were decomposed into three Gaussian peaks proportional to $\exp[-(Q_0 - Q)^2 / (\Delta Q)^2]$. d_{002} is estimated interlayer spacing from Q_0 , and α is thermal-expansion coefficient.

Peak	298 K			873 K			α ($10^{-5}/\text{K}$)
	Q_0 (1/Å)	d_{002} (Å)	ΔQ (1/Å)	Q_0 (1/Å)	d_{002} (Å)	ΔQ (1/Å)	
A	1.836	3.422	0.0091	1.809	3.473	0.0091	2.6
B	1.846	3.403	0.035	1.820	3.452	0.038	2.5
C	1.831	3.432	0.083	1.815	3.462	0.0944	1.6

mated as 41% of peak C. The second model is that MWNT has a mixed structure of the Russian doll tubules and the highly defective tubules. One of this type of structure has been reported by Amelinckx *et al.*,¹⁰ which is a mixed structure of Russian doll and jellyrolled tubules as shown in Fig. 1(c).

We can also propose another structural model for the mixed-type MWNT. In this model, the outer region of MWNT is made up of polyhedron graphite consisting of graphitized flat domains, while the inner region has a Russian-doll-type nested structure consisting of the seamless circular tubules, as illustrated in Fig. 1(d). The polygonal cross section has been suggested by a detailed XRD analysis¹⁸ and a TEM observation,¹⁹ and also observed by SEM (Ref. 20) in the thick MWNT's. The flat graphene sheets in the graphitized domains may not be connected to those in the neighboring domains at the ridges. Even in the connected polygonal graphite, the polyhedron would be weaker at the ridges than at the flat graphitized regions. Thus, for example, high-temperature treatments in oxygen or hydrogen atmosphere would easily divide the polyhedron into the several flat small sheets at the ridges.

Finally we discuss the tube diameters (the number of layer N). In principle, the domain size (N) can be deduced from the (002) and (004) reflections by separating the domain size broadening and the strain broadening. In the present case, however, we could just obtain the lower limit for peaks A and B because the strain broadening dominates the observed linewidth; $N > 200$ and > 38 for peaks A and B, respectively. On the other hand, for peak C, N was found to be most probable between 7 and 15. These estimates are reasonably consistent with the TEM images of the present sample that exhibited the existence of a lot of thin MWNT's

with N of around 10, as well as the existence of the very thick MWNT's with outer diameters more than 1500 Å corresponding to peak A. Therefore, combined with the small thermal expansion for peak C, it can be concluded that a large amount of the thin tubes is the closed nested tubule structure. With increasing N , however, the graphitization may occur. This results in polygonal deformations and a shortening of the d spacing, consistent with the present results (Table I); peaks A and B have shorter interlayer distances than peak C. Because the ridges may be defected during arc discharge, the majority of the tubules in single thick MWNT would not have closed circular structure, exhibiting the large d -spacing thermal expansion.

In conclusion, it was found that the XRD peak consists of at least three components (peaks A, B, and C) with the quite different peak width. Peak C has an average interlayer thermal-expansion coefficient α of $1.6 \times 10^{-5} \text{ K}^{-1}$, much smaller than $2.6 \times 10^{-5} \text{ K}^{-1}$ for peaks A, B, and the graphite peaks. This observation indicates the existence of both the closed Russian doll MWNT and the highly defective MWNT. The closed Russian doll MWNT is assigned to the thin MWNT's with typically 7–15 tubules. In contrast, the larger diameter tubes are highly defective. Because the apparent peak position for the (00 l) reflection is dominated by the thick MWNT's, it could not provide the correct information on the structural properties of thin MWNT's.

Authors thanks to Dr. Mukul Kumar for critical reading of the manuscript. Y.M. gratefully acknowledges Professor Y. Tajima for valuable comments. This work was supported in part by the Grant-in-Aid for Scientific Research on the Priority Area "Fullerenes and Nanotubes" by the Ministry of Education, Science, Sports and Culture of Japan.

¹S. Iijima, *Nature (London)* **354**, 56 (1991).

²For reviews, see P. J. F. Harris, *Carbon Nanotubes and Related Structures* (Cambridge University Press, Cambridge, 1999); M. S. Dresselhaus, G. Dresselhaus, and P. C. Eklund, *Science of Fullerenes and Carbon Nanotubes* (Academic Press, New York, 1995).

³S. Iijima and T. Ichihashi, *Nature (London)* **363**, 603 (1993).

⁴D. S. Bethune, C. H. Kiang, M. S. de Vries, G. Gorman, R. Savoy, J. Vazquez, and R. Beyers, *Nature (London)* **363**, 605 (1993).

⁵J. Yu, R. K. Kalia, and P. Vashishta, *J. Chem. Phys.* **103**, 6697 (1995).

⁶A. M. Rao, E. Richter, S. Bandow, B. Chase, P. C. Eklund, K. A. Williams, S. Fang, K. R. Subbaswamy, M. Menon, A. Thess, R. E. Smally, G. Dresselhaus, and M. S. Dresselhaus, *Science* **275**, 187 (1996).

⁷J. W. G. Wildoer, L. C. Vennema, A. G. Rinzler, R. E. Smalley, and C. Dekker, *Nature (London)* **391**, 59 (1998).

⁸T. W. Odom, J. L. Huang, P. Kim, and C. M. Lieber, *Nature (London)* **391**, 62 (1998).

⁹O. Zhou, R. M. Fleming, D. W. Murphy, C. H. Chen, R. C. Haddon, A. P. Ramirez, and S. H. Glarum, *Science* **263**, 1744

(1994).

¹⁰S. Amelinckx, D. Bernaerts, X. B. Zhang, G. Van Tendeloo, and J. Van Landuyt, *Science* **267**, 1334 (1995).

¹¹S. Bandow, *Jpn. J. Appl. Phys., Part 2* **36**, L1403 (1997).

¹²X. Zhao and Y. Ando, *Jpn. J. Appl. Phys., Part 1* **37**, 4846 (1998).

¹³H. Kataura, Y. Achiba, X. Zhao, and Y. Ando, *MRS Proceedings* No. 593 (2001), pp. 113–118.

¹⁴X. Zhao, M. Ohkohchi, M. Wang, S. Iijima, T. Ichihashi, and Y. Ando, *Carbon* **35**, 775 (1997).

¹⁵L. C. Qin, X. Zhao, K. Hirahara, Y. Miyamoto, Y. Ando, and S. Iijima, *Nature (London)* **408**, 50 (2000).

¹⁶B. E. Warren, *Phys. Rev.* **59**, 693 (1941).

¹⁷R. K. Kirby, T. A. Hahn, and B. D. Rothrock, *American Institute of Physics Handbook*, edited by D. E. Gray (McGraw-Hill, New York, 1972), 3rd ed.

¹⁸D. Reznik, C. H. Olk, D. A. Neumann, and J. R. D. Copley, *Phys. Rev. B* **52**, 116 (1995).

¹⁹C.-H. Kiang, M. Endo, P. M. Ajayan, G. Dresselhaus, and M. S. Dresselhaus, *Phys. Rev. Lett.* **81**, 1869 (1998).

²⁰Y. Gogotsi, J. A. Libera, N. Kalashnikov, and M. Yoshimura, *Science* **290**, 317 (2000).